TH/1-6

Instability and Transport Driven by an Electron Temperature Gradient Close to Critical

J.Q. Dong 1), G.D. Jian 1), A.K. Wang 1), H. Sanuki 2), and K. Itoh 2)

1) Southwestern Institute of Physics, Chengdu, China
2) National Institute for Fusion Science, Toki, Japan

e-mail contact of main author: jqdong@chungtze.ps.uci.edu

Abstract Electron temperature gradient (ETG) driven instability in toroidal plasmas is studied with gyrokinetic theory. The full electron kinetics is considered. The upgraded numerical scheme for solving the integral eigenvalue equations allows the study of both growing and damping modes, and thus direct calculation of critical gradient. Algebraic formulas for the critical gradient with respect to ratio of electron temperature over ion temperature and to toroidicity are given. An estimation for turbulence induced transport is presented.

1. Introduction

Recent observations on tokamaks have shown that, within internal transport barriers (ITBs), electron thermal transport hardly changes while ion thermal diffusivity is reduced to the neoclassical level. These findings support the hypothesis that, within an ITB, ion temperature gradient turbulence is suppressed by $\mathbf{E} \times \mathbf{B}$ shear flow, whereas electron temperature gradient (ETG) turbulence controls electron transport. As a result, ETG instability and anomalous electron thermal transport have received intensive research attention in recent years.

The critical temperature gradients for instabilities and the turbulent electron thermal transport in the parameter regimes close to critical temperature gradients have been studied in detail in experiments. [1] It seems apparent that critical gradient is one of the few physics quantities for which results from the linear theory may be compared quantitatively with experimental observations. Therefore, a precise identification of critical gradients both experimentally and theoretically is of great importance in the study of the instability and the turbulent transport.

The ETG driven instability and turbulent transport in toroidal plasmas are studied with gyrokinetic theory in this work. The full electron kinetics is considered. The behavior of the modes and the transport in the parameter regimes close to the threshold of the instability are emphasized.

2. Physical models and eigenmode equations

An axis symmetric toroidal geometry with circular flux surfaces is employed. The curvature and magnetic gradient effects $\omega_D(v_\perp^2, v_\parallel^2, \theta)$ of electrons are included. The ballooning

representation is used. The full electron transit $k_\parallel v_\parallel$ and finite Larmor radius effects are retained. Electron bouncing is neglected and ion response is adiabatic. The integral dispersion equation for low β(= plasma pressure/magnetic pressure) plasmas obtained from Poisson's equation is as follows: [2]

$$\left[1+\tau_i+\frac{k_\perp^2}{2}\frac{\Omega_e^2}{\omega_{pe}^2}\right]\widehat{\phi}(k)=\int_{-\infty}^{+\infty}\frac{dk'}{\sqrt{2\pi}}K(k,k')\widehat{\phi}(k'), \tag{1}$$

where $\widehat{\phi}(k)$ is the extended Fourier component (in ballooning space) of the perturbed potential $\tilde{\phi}$, and

$$K(k,k')=-i\int_{-\infty}^{0}\omega_{*e}d\tau\sqrt{2}\,e^{-i\omega\tau}\frac{\exp\left[-\frac{(k'-k)^2}{4\lambda_e}\right]}{\sqrt{a}_e\,(1+a_e)\sqrt{\lambda_e}}\times\left\{\frac{\omega}{\omega_{*e}}-1+\frac{3}{2}\,\eta_e-\frac{2\eta_e}{(1+a_e)}\times\right.$$

$$\left.\left[1-\frac{k_\perp^2+k_\perp'^2}{2(1+a_e)}+\frac{k_\perp\,k_\perp' I_1}{(1+a_e)I_0}\right]-\frac{\eta_e(k-k')^2}{4a_e\lambda_e}\right\}\Gamma_0(k_\perp,k_\perp'), \tag{2}$$

with

$$\lambda_e=\frac{\tau^2\omega_{*e}^2}{a_e}\left(\frac{\widehat{s}}{q}\epsilon_n\right)^2,\qquad a_e=1-i2\epsilon_n\omega_{*e}\tau\frac{g(\theta,\theta')}{(\theta-\theta')},$$

$$g(\theta,\theta')=(\widehat{s}+1)(\sin\theta-\sin\theta')-\widehat{s}(\theta\cos\theta-\theta'\cos\theta'),$$

$$k=k_\theta\widehat{s}\theta,\quad k'=k_\theta\widehat{s}\theta',\quad \omega_{pe}^2=\frac{4\pi ne^2}{m_e},\quad \Omega_e=\frac{eB}{m_ec},$$

$$\Gamma_0=I_0\left(\frac{k_\perp\,k_\perp'}{(1+a_e)}\right)\exp\left[-(k_\perp^2+k_\perp'^2)/2(1+a_e)\right],$$

$$k_\perp^2=k_\theta^2[1+(\widehat{s}\theta)^2],\qquad k_\perp'^2=k_\theta^2[1+(\widehat{s}\theta')^2],$$

$$\omega_{*e}=\frac{cT_ek_\theta}{eBL_n},\quad \epsilon_n=\frac{L_n}{R},\quad \eta_e=\frac{L_n}{L_{Te}},\quad \tau_i=\frac{T_e}{T_i},$$

The quantities k, k' and k_θ are normalized to $\rho_e^{-1}=\Omega_e/v_{te}=eB/c\sqrt{2T_em_e}$. I_j is the modified Bessel function of order $j=0,1$. L_n is the density gradient scale length, L_{Te} is the electron temperature gradient scale length, q is the safety factor, and $\widehat{s}=rdq/qdr$ is the magnetic shear. The third term on the left side of Eq. (1) represents the Debye shielding effect, which is significant for short wavelength modes of $k_\perp\lambda_D\gtrsim 1$, with λ_D being the Debye length.

3. Numerical Results

The integral equation, Eq. (1), has to be solved numerically. The procedure for solving such equations is well documented and the computer code HD7 [2] for solving the equations is upgraded by introducing a new integration scheme in this work. The integration over τ in Eq. (2) does not converge for damped modes with negative growth rate if it is performed along the real axis. This is in line physically with the causality condition . On the other

hand, however, it is proved in Ref. [3] that an analytical continuation of the integration into a complex τ-plane will not change the results of the integration and allows it to converge for a negative growth rate.

For the numerical results given in this work, we transform the real τ integration into an integration in a complex τ-plane with [3]

$$\tau = \begin{cases} -(1+i|\omega|s)s, & \omega_r > 0, \\ -(1-i|\omega|s)s, & \omega_r < 0, \end{cases} \tag{3}$$

where s $(0 \leq s < \infty)$ is a real integration variable.

The new numerical scheme allows not only the growing modes but also the damping modes to be investigated. Therefore, the critical gradients are calculated with precision, for the first time, without extrapolation. The parameters for the numerical results given here are $\widehat{s} = 1$, $q = 1.5$, $\tau_i = 1$, $d_s = \Omega_e^2/\omega_{pe}^2 = 0$ and $\epsilon_n = 0.2$ unless otherwise stated.

A. Critical gradient versus temperature ratio

Given in Fig. 1 are the maximum growth rate of the mode (with respect to k_θ) (a) (for $\tau_i = T_e/T_i = 0.5$, 0.75, 1, 1.5, 2, 3, 4 and 5) and the critical gradient $(R/L_{Te})^{ct}$ (b) versus η_e and τ_i, respectively.

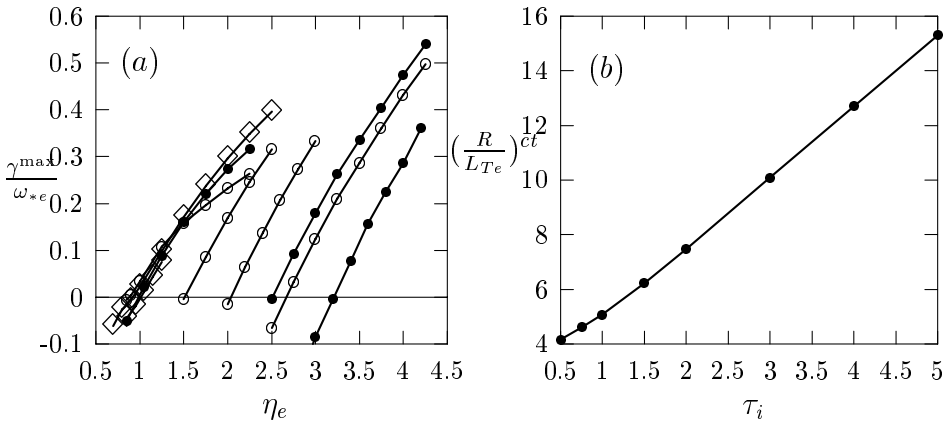

FIG.1. Maximum growth rate (a) *and critical gradient* (b) versus η_e and τ_i.

It is explicit that, in the stability boundary region, the maximum growth rate is an offset linear function of η_e,

$$\gamma^{max} = \sigma_1(\tau_i)\omega_{*e}(\eta_e - \eta_e^{ct}) = \sigma_1(\tau_i)\omega_{*e}\epsilon_n[\frac{R}{L_{Te}} - (\frac{R}{L_{Te}})^{ct}]. \tag{4}$$

The relation of $(R/L_{Te})^{ct}$ versus τ_i shown in Fig. 1(b) may be approximated as

$$(\frac{R}{L_{Te}})^{ct} = \begin{cases} 3.5 + 1.07\tau_i + 0.5\tau_i^2, & 0.5 \leq \tau_i \leq 1.5, \\ 2.35 + 2.59\tau_i, & 1.5 \leq \tau_i \leq 5.0. \end{cases} \tag{5}$$

The function $\sigma_1(\tau_i)$ with the other parameters fixed is given in Fig. 2, where the points are numerical results while the curve is from the fitting function,

$$\sigma_1 = \frac{1}{0.0173\tau_i^2 + 1.95\tau_i + 1,18}. \tag{6}$$

The fitting is excellent.

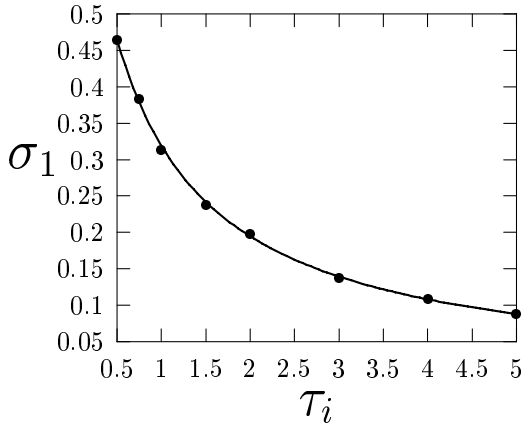

FIG.2. Proportionality factor σ_1 versus τ_i.

B. Critical gradient versus toroidicity

The same threshold gradient searching is performed for varying ϵ_n and fixed τ_i' as was done above for a fixed ϵ_n and varying τ_i. The maximum growth rate may also be presented as

$$\gamma^{max} = \frac{\sigma_2(\epsilon_n)}{\epsilon_n}\omega_{*e}(\eta_e - \eta_e^{ce}) = \sigma_2(\epsilon_n)\omega_{*e}[\frac{R}{L_{Te}} - (\frac{R}{L_{Te}})^{ce}]. \tag{7}$$

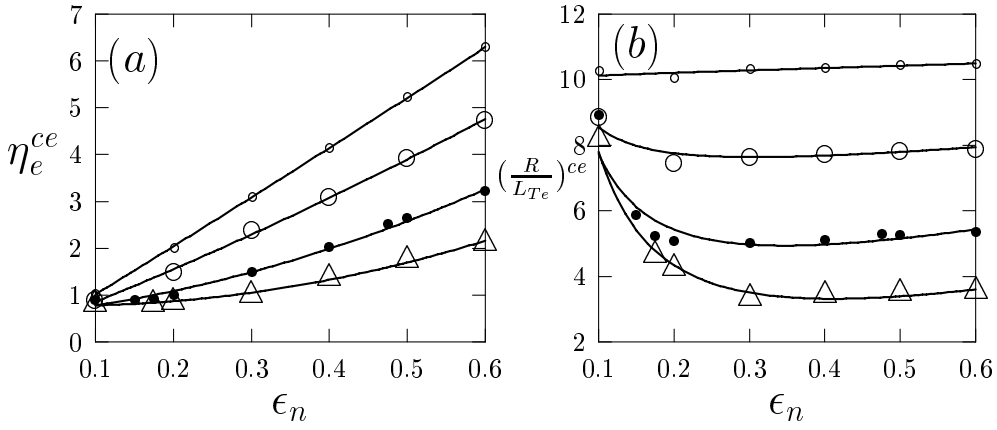

FIG. 3. Critical gradient parameters η_e^{ce} (a) and $(\frac{R}{L_{Te}})^{ce}$ (b) versus ϵ_n.

The critical gradient parameters η_e^{ce} and $(\frac{R}{L_{Te}})^{ce}$ obtained are shown in Fig. 3 for $\tau_i = 3$ (small open circles), 2 (large open circles), 1 (closed circles) and 1/3 (triangles). Here, the

points are the numerical results and the curves are from the fitting functions,

$$\eta_e^{ce} = \begin{cases} 4.688\epsilon_n^2 - 0.5218\epsilon_n + 0.7855, & \tau_i = \frac{1}{3}, \\ 4.607\epsilon_n^2 + 1.747\epsilon_n + 0.5525, & \tau_i = 1, \\ 2.104\epsilon_n^2 + 6.346\epsilon_n + 0.1985, & \tau_i = 2, \\ 0.679\epsilon_n^2 + 10.09\epsilon_n - 0.0040, & \tau_i = 3, \end{cases} \tag{8}$$

and

$$(\frac{R}{L_{Te}})^{ce} = \frac{\eta_e^{ce}}{\epsilon_n}, \tag{9}$$

with η_e^{ce} given by Eq. (8). The proportionality factor $\sigma_2(\epsilon_n)$ is given in Fig. 4, where the points are from the numerical results while the curves are from the fitting function,

$$\sigma_2(\epsilon_n) = \begin{cases} 1.039\epsilon_n - 0.0780, & \tau_i = \frac{1}{3}, \\ 0.432\epsilon_n - 0.0182, & \tau_i = 1, \\ 0.253\epsilon_n - 0.0101, & \tau_i = 2, \\ 0.176\epsilon_n - 0.0076, & \tau_i = 3. \end{cases} \tag{10}$$

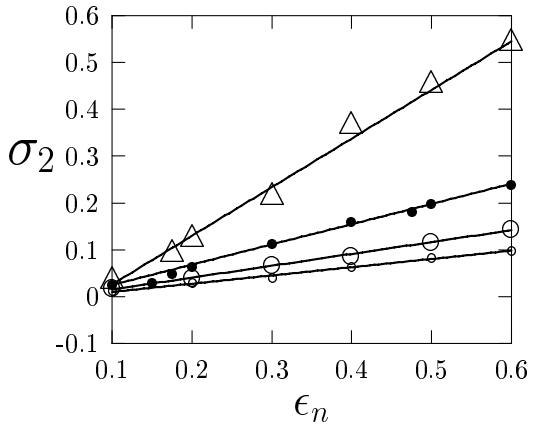

FIG. 4. Proportionallity factor σ_2 versus ϵ_n.

4. Conclusion and discussion

The experimental studies of electron transport were reviewed in Ref. [1], where the thresholds $(R/L_{Te})^c$ from seven tokamaks (COMPASS-D, RTP, TCV, FT-U, AUG, Tore Supra and JET) were reported to be between 8 and 12. The values given in Figs. 1 and 3 are lower and close to the experimental observations except for very high $\tau_i(> 4)$. In particular, the experiments on ASDEX-Upgrade clearly show that there is a threshold of electron temperature gradient $(\nabla T_e)^c$ above which the transport increases strongly to keep the profiles close to $(\nabla T_e/T_e)^c$. (The experimentally measured stiffness of the profiles is a consequence of this fact.) In addition, the experimentally measured critical gradient is $(\nabla T_e/T_e)^c \sim 6/\mathrm{m}$. [1] Considering that the major radius of the device is 1.65 m, we get $(R/L_{Te})^c \sim 9.9$, which corresponds to $\tau_i \sim 3$ in Fig. 1, where we take $\epsilon_n = 0.2,\ q = 1.5$, and $\hat{s} = 1.0$. Meanwhile,

the threshold $(R/L_{Te})^c \sim 9.9$ corresponds to $\epsilon_n < 0.1$ and $\epsilon_n \lesssim 0.2$ in Fig. 3 for $\tau_i < 3$ and $\tau_i \sim 3$, respectively. Similarly, in the case of Tore Supra, the experiments indicate that $(R/L_{Te})^c \sim 12$ for $\widehat{s}/q \sim 0.67$ [1]. This also corresponds to $\tau_i \sim 3.7$ in Fig. 1 and $\tau_i > 3$ in Fig. 3. Because the parameters ϵ_n, q, τ_i and $\widehat{s}$ for the experiments are not available, we do not attempt to claim the agreement of our results with the experiments. However, the fact that the theoretical results fall right inside the range of experimental observations is certainly not coincidental. At least, this is strong support for the claim that the turbulence and turbulent transport observed in the experiments are driven by the toroidal ETG modes.

Substituting Eq. (6) into Eq. (4), we have

$$\gamma^{max} \simeq 0.38 \frac{c k_\theta^{max} T_i}{eBR} [\frac{R}{L_{Te}} - (\frac{R}{L_{Te}})^{ct}]. \tag{11}$$

The experimental data from Ref. [1] clearly indicate that the normalized electron thermal diffusivity $\chi_e/T_e^{1.5}$ versus $(\nabla T_e/T_e)$ exhibits universal behavior for plasmas under different discharge conditions. Here, the factor $1/T_e^{1.5}$ cancels the gyro-Bohm scaling of χ_e with T_e. Therefore, the mixing length estimation for the transport, $\chi_e \sim \gamma^{max}\Delta^2$, seems a good approximation since the universality of $\chi_e/T_e^{1.5}$ observed in the experiments is nothing but that of γ^{max} given in Eqs (4) and (9). On the other hand, assuming $\Delta \sim c/\omega_{pe} \sim 1/k_\theta^{max}$, we may get

$$\chi_e \sim \frac{D_B}{0.0173\tau_i^2 + 1.95\tau_i + 1,18} \frac{c}{\omega_{pe}} [\frac{1}{L_{Te}} - (\frac{1}{L_{Te}})^{ct}] \mathrm{F}(\epsilon_n, \widehat{s}, q), \tag{12}$$

for $L_T \leq L_{Te}^{ct}$ with

$$D_B = \frac{cT_e}{eB} \quad \text{and} \quad \mathrm{F}(\epsilon_n, \widehat{s}, q)$$

being the diffusion coefficient defined by Bohm and an order unity function of the rest parameters, respectively.

Similar results for χ_e may also be obtained from Eqs (7) and (10).

This work is partly supported by the National Natural Science Foundation of China, Grant No. 10135020, and the Nuclear Science Foundation of China, Grant No. Y7100C0301.

References

[1] F. Ryter, *et al.*, Plasma Phys. Control. Fusion **43** (2001) A323.
[2] J.Q. Dong, *et al.*, Phys. Fluids B **4** (1992) 1867.
[3] H. Sugama, Phys. Plasmas **6** (1999) 3527.